Foundations for Smart Metamaterials by Liquid Metal Digital Logic and Magnetoelastic Properties Control

Master's Thesis

Presented in Partial Fulfillment of the Requirements for the Degree Master of Science in the Graduate School of The Ohio State University

By

Zachary Nick

Graduate Program in Aeronautical and Astronautical Engineering

The Ohio State University

2020

Thesis Committee

Ryan L. Harne, Advisor

Marcelo J. Dapino, Advisor

Abstract

This research investigates the strategic design of elastomeric metamaterials to induce controllable mechanical properties and sensing capabilities. Elastomers have been utilized in the creation of flexible electronics due to the inherent ability to nondestructively deform. When a malleable, conductive material, such as liquid metal, is incorporated into an elastomeric host structure, a flexible electronic material is created that may maintain electrical conductivity during high strain loading. While research has uncovered ways of utilizing deformation of flexible electronics to achieve functionality such as resistance change and self-healing, there are few studies that explore mechanical and electrical properties of such systems when subjected to compression. The material responses may be made more versatile by exploiting principles of elastic metamaterials. Such metamaterials contain void architectures that create elastic truss networks capable of reversible buckling, and have shown ability to provide impact and vibration attenuation capabilities. Methods of controlling the mechanical properties of these metamaterials, such as functionally grading layers of beams, or incorporating magnetic microparticles into the elastomer matrix to modify the stiffness in real-time with an externally applied magnetic field, have been explored. Yet, research is lacking on the interplay of design parameters and magnetic field that result in mechanical behaviors. Motivated by these needs, this research explores foundations of new generations of smart

metamaterials by establishing methods for sensing and control of material behavior. A new approach to liquid metal-based sensing in elastomeric materials is built up, leveraging mechanical deformation to induce a digital logic sensing modality. Then, the interplay of mechanical design and magnetoelasticity is explored for metamaterials with properties governed by ferromagnetic particle filler and the presence of magnetic field. The findings advance the state-of-the-art of smart metamaterials, and may be combined in future research endeavors to create self-sensing, self-tuning, autonomous material systems.

Dedication

For those who have continued to prop me up.

Acknowledgments

I would like to thank my advisor, Dr. Ryan L. Harne, for his unwavering guidance and support both in and out of academia.

I would like to thank my advisor, Dr. Marcelo J. Dapino, for his knowledgeable guidance and support in my academic pursuits.

I would like to thank the members of the Air Force Research Laboratory Materials and Manufacturing Directorate (RX) for sharing knowledge and resources pertaining to flexible electronics.

Table of Contents

List of Tables

List of Figures

Chapter 1. Introduction

In this chapter an overview of elastomeric metamaterials, magnetorheological elastomers, flexible electronics, and state-of-the-art applications thereof are explored. Then, having identified needs in the multiple scientific fields, the objectives of this research to establish sensing and control approaches for smart metamaterials are articulated. The organization of this thesis is then presented.

1.1 Literature review

1.1.1 Elastomeric metamaterials and magnetorheological elastomers

Elastomeric materials are often a foundation for mechanical metamaterials, which derive unique properties relative to the microstructure composition, such as exploiting internal truss networks featuring reversible buckling [1]. Numerous elastomeric metamaterials are shown to exhibit negative Poisson's ratio through the collapse of internal truss structures [2] [3]. Furthermore, these reversible buckling beams have shown promising ability to provide exceptional shock, impact, and elastic energy dissipation [4] [5] [6] [7] [8] [9]. Parameters of the beam networks, such as functionally grading the beam thickness, can help dictate and control the mechanical properties and collapse of the structure [10]. This controllability provides the opportunity to tune mechanical properties of lightweight elastomeric materials.

Elastomers have also been used to create magnetorheological elastomers (MRE) through the incorporation of magnetic microparticles into an elastomer matrix [11] [12] [13]. When analyzed within an externally applied magnetic field, the MRE is subject to material property changes [14], while also being able to instill differing mechanical properties purely through microparticle orientation, even outside of an external magnetic field. The proximity and poling direction of these microparticles within the matrix may increase internal forces within the MRE due to a stronger magnetic effect [15]. Applications such as MRE capable of quickly transforming into 3D shapes and moving through external field activation may be used in medical fields for remote drug dose administration [16]. Methods of further reinforcing mechanical and magnetic properties within MRE include incorporating multiwall carbon nanotubes or carbon black, which can also improve the bonding between magnetic microparticles and the elastomer matrix [17] [18].

While the state-of-the-art has shown great promise in adaptable mechanical properties, these new findings do not fully utilize multiple available methods of controlling collapse to induce mechanical property changes at once. Furthermore, such systems are unable to self-sense to enable the possibility to self-tune. If a metamaterial system were to be created that further scrutinized multiple structural design parameters, including their combination thereof, and how they influence collapse, even further fine-tuning may be achievable. If this same system were to incorporate magnetoelastic properties with self-sensing functionality, an autonomous structure capable of self-tuning through nonuser corrective feedback may be possible.

1.1.2 Flexible Electronics

Another implementation of elastomers that takes advantage of the inherent flexibility are flexible electronics. Flexible electronics incorporate nonrigid properties of elastomers and conductive materials capable of nondestructively deforming to create applications in soft robotics, wearable technologies, and beyond [19] [20] [21] [22]. A popular choice of conductive material interfaces within an elastomer substrate for flexible electronic systems that is capable of conforming under stress are gallium-based liquid metal alloys [23] [24] [25]. These gallium-based liquid metals react with air to almost instantaneously create nonconductive oxide surface layers which has fueled research on how to mitigate, or take advantage of, such unique mechanical and electrical insulating properties [26] [27] [28]. Such discoveries have led to applications such as liquid metal-elastomer composites possessing autonomous healing capabilities upon being subjected to damaging loads [29] [30].

These state-of-the-art advancements lay groundwork for a new idea of incorporating electrically conductive inclusions into light weight elastomeric metamaterial systems. Recent research has in face given first demonstration of a combination of such constituents, namely utilizing Ag-TPU (silver-thermoplastic polyurethane) conductive traces to achieve modifiable conductive properties during compressive loading of elastic metamaterials [31] [32]. Yet, such a system simply alters resistance as the system is strained rather than exhibiting an off-on switching functionality. Prior research has investigated the effects of torsional, tensile, and bending stresses, yet utilization of compressive strain for electrical functionality is lacking [19]. Investigating liquid metal-

filled microchannels within elastomeric metamaterials under compressive loading may advance the state-of-the-art by uncovering behavior not yet characterized, such as the reversible switching off and on of conduction while maintaining the reversible mechanical property changes inherent in elastomeric metamaterials. Such multifunctionality may be leveraged to provide digital logic capabilities that, when paired with a system capable of self-tuning, may lay the foundation for a novel, autonomous flexible electronic metamaterial system.

1.2 Objective of thesis

The utilization of liquid metal in elastomeric metamaterials may result in multifunctional materials capable of acting as sensors while concurrently providing tunable mechanical properties. To build a foundation for such potential, methods to exploit liquid metal-filled metamaterials must be established. Such an approach will guide the first methods to correlate instantaneous mechanical behavior to the conductivity properties of the whole *flexible electronic metamaterial*. To formulate techniques to control the mechanical behavior, techniques for the simultaneous design of microstructure and usage of magnetic microparticles must be identified to uncover synergistic methods to control metamaterial response. Investigating these *smart* capabilities of metamaterials would create essential groundwork for future fundamental research on generations of smart metamaterials with integrated sensing and control mechanisms.

This research aims to advance the state-of-the-art in the fields of flexible electronics and magnetoactive metamaterials by studying concurrent implementation of mechanical

metamaterial design with either flexible electronic materials or magnetoactive materials for sensing and control mechanisms, respectively. The research objectives of this thesis are as follows:

1. Develop a method of incorporating liquid metal-filled microchannels into an elastomeric metamaterial to create a flexible electronic system that utilizes reversible mechanical collapse as a means to modify conductive state.
2. Investigate electrical and mechanical properties of the flexible electronic material by uncovering relationships between structural and microchannel deformation and conductivity to identify sensing capabilities.
3. Analyze the influence of multiple structural design parameters and applied magnetic fields on magnetoelastic metamaterials for controllable mechanical property adaptation.

The first objective aims to manifest an elastomeric metamaterial system containing liquid metal-filled microchannels that, under compressive loading, may experience changes in conductive properties during loading and unloading. This will provide a foundation from which the multifunctionality may be explored.

Once realized, such a system may be scrutinized to better understand the underlying multifunctional interplay between the collapse of the host structure and the resulting collapse of the embedded microchannel that may identify loading thresholds. With the use of a conductive liquid metal sensitive to forming nonconductive surface layers when exposed to air, methods of extending functionality are explored and defined.

Taking advantage of the inherent reversibility of elastic beam buckling, combinations of structural design parameters that may influence critical points of collapse, such as force and strain, are investigated. Following structural parameter studies, MRE principles are incorporated to create a highly tunable material capable of controlling the mechanical property adaptation through external magnetic fields.

1.3 Organization of thesis

This thesis is organized in the proceeding chapters in the following manner.

Chapter 2 demonstrates the capability and utility of incorporating liquid metal-filled microchannels into elastomeric metamaterial structures. The following research will uncover the relationships between embedded microchannels and host structures, and the resulting effects on conductive state switching for sensing functionality. To maintain functionality through multiple switching of conduction states, methods of extending conductive lifecycle through iterative loadings are illuminated.

Chapter 3 investigates the influence of structural design parameters of a stacked metamaterial system on collapse and the resulting mechanical property changes. Different levels of vertical beam thickness and offset are analyzed both independently, and in various combinations, to uncover the range of tunable collapse through simple parametric modifications. Another layer of in situ tunability through the incorporation of magnetic microparticles into the elastomer matrix is explored inside and outside of an external magnetic field to create a highly tunable material system with controllable mechanical properties.

Chapter 4 summarizes the findings uncovered in this research and proposes avenues for future research involving smart metamaterials and the discoveries herein.

Chapter 2. Liquid Metal Microchannels as Digital Sensors in Mechanical Metamaterials

Flexible electronics offer impeccable opportunities for diversifying applications of circuitry in future developments across a multitude of fields. The invaluable ability to nondestructively deform, unlike prototypical rigid counterparts, while maintaining conductivity accentuates the inherent benefits. Likewise, lightweight elastomeric materials contain the extraordinary ability to have tunable mechanical properties for a variety of vibration attenuation applications. This work combines these principles to create a flexible electronic metastructure capable of changing conduction and stiffness states during loading and unloading. This is achieved by embedding a liquid metal-filled microchannel within an elastomer with integrated void architectures to induce tunable collapse of both the structure and the microchannel, thereby disconnecting the continuous contact of liquid metal, when compressed. It is found that both the microchannel diameter and the host structure it is embedded within affect the stress required to temporarily terminate conduction. The investigation of lifecycle extendibility for conduction switching also finds that longer lifecycles are achieved through prewashing microchannels with NaOH emulsion prior to liquid metal injection, and by employing larger microchannel sizes. Finally, a stacked multichannel metastructure displays the traits of a multistep sensor capable of multiple mechanical property changes. These

discoveries may motivate future applications requiring flexible power delivery, sensing, and vibration isolation.

2.1 Introduction

Flexible and stretchable electronic materials establish essential foundation for future wearable technologies, soft robots, and more [20] [33] [34] [35] [22] [36] [21] [19]. Gallium-based liquid metals have seen a recent surge of attention due to increased conformability of the liquid phase when synthesized with elastomeric substrates or host matrices [30] [37] [24] [23] [28] [25] [26] [27]. Strategic use of liquid metal substrates and surfaces moreover creates opportunity for stress-activated functionality, such as via polymerized liquid metal networks [38] or liquid metal-elastomeric materials [39]. This opportunity to leverage an integration of elastomeric matrix and liquid metal inclusions has uncovered unique self-healing functionality in liquid metal-elastomer composites when subjected to damaging stresses [29]. Such advancements in flexible materials invested with liquid metal suggest extraordinary opportunity for electrically and mechanically functional platforms [40] to be explored in a diverse range of future applications.

Substantial research focus on liquid metal-based flexible electronics has given attention to conductivity sustained during tensile, torsional, and bending stresses [19]. Yet, flexible electronic materials may be subjected to compressive loads that could be damaging to the whole material system. In such case, fundamental approaches must be investigated to extend material functionality for sustained electrical operation while providing elastic

energy dissipation that sustains the system [4] [8] [7] [6] [5]. These latter capabilities are often achieved by utilizing the inherent reversibility of elastic beam buckling [1]. Sears et al. [32] [31] demonstrated the first combination of such principles using Ag-TPU conductive traces (silver-thermoplastic polyurethane) on TPU metamaterial structures that combined smooth change of conductivity properties according to applied compressive stresses. The smoothly varying conductivity of the Ag-TPU materials [32] [31] provides first evidence of merging metamaterial mechanics with stretchable electronic materials yielding an analog mode of electrical function. On the other hand, digital operations are the language of many electronic devices that may interface with the conductive materials. This encourages formulation of flexible electronic materials that may change conductivity in discrete modes. By establishing a method of integrating liquid metal networks within mechanical metamaterials where metamaterial deformation results in discrete change of conductivity, new fundamental concepts of digital logic governed by metamaterial mechanics may be formulated.

Motivated by such opportunities, this chapter investigates a multifunctional metamaterial concept that yields digital electrical signaling in response to smooth, continuous metamaterial compressive deformation of buckling members. These functionalities are realized simultaneously by introducing void architectures into a bulk elastomer of constant cross-section with a centrally located liquid metal microchannel, Figure 1. The triangular voids form an X-shaped beam network, similar to the embodiment of metamaterial studied by Bunyan and Tawfick [41] and El-Helou and Harne [10]. A central elastomer ligament passes through the center of the X shape, through which runs a

liquid metal-filled microchannel. When compressed, the beam network rotates about the center, leading to a pinching action on the microchannel containing the liquid metal, as shown in Figure 1a. This constriction of liquid metal terminates the conduction through the microchannel, creating an open circuit. This behavior is shown in Figure 1b,c where a series connection of the metamaterial unit with an LED matrix turns off the lights once the liquid metal is constricted due to metamaterial compression. When the load is removed, the liquid metal may recoalesce at the pinched region and close the circuit to recover the electrical functionality.

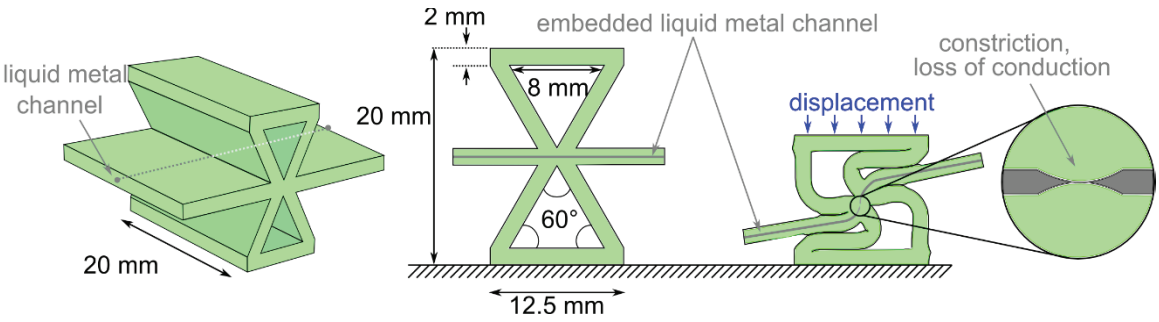

Figure 1. (a) Isometric and cross-sectional views of metamaterial unit cell detailing compression mechanism for channel constriction, (b) lights powered through the unit cell connected in series creating a closed circuit, and (c) lights switched off by opening the circuit through collapse of the structure and microchannel.

This chapter studies the liquid metal metamaterial unit to identify the mechanisms involved to induce and control the discrete electrical conductivity behavior observed in the preliminary example of Figure 1. Having established an understanding of the parametric influences governing the electrical operation, the unit is tiled into a periodic

and functionally graded metamaterial to test the working principles observed at the unit level in relation to mechanisms of digital operation at the scale of a material system. The chapter concludes with a summary of discoveries achieved in this research and trajectories of continuing research to be explored.

2.2 Fabrication and Experimental Methods

Throughout this study, the metamaterials and units are fabricated by first casting silicone rubber into 3D printed molds. Acrylonitrile butadiene styrene (ABS) filament is used for the 3D printed (FlashForge Creator Pro) mold negatives. Polymer wire is stretched taut through passages in the molds to create the microchannels. Platinum cure silicone rubber (Smooth-On Mold Star 15S, Macungie, Pennsylvania) is then cast in the mold, and the manufacturer-recommended 4-hour cure time is allowed to pass in atmospheric room conditions prior to demolding. Upon demolding the silicone rubber from the mold, the polymer wire is extracted to reveal a hollow microchannel within the elastomer sample. A syringe with 22-gauge needle is used to inject sodium hydroxide (NaOH, 0.1M) through the empty microchannel. The influence of the NaOH is studied in latter portions of this chapter, and at this stage of fabrication results in a coating of the microchannel walls with NaOH to impede the liquid metal oxidation. Another syringe then injects liquid metal (Galinstan, GaInSn, Rotometals, San Leandro, California) into the microchannel. Copper wire of 34 gauge is inserted into each microchannel end before sealing the microchannel with additional silicone rubber. The specimen is aerated for 24 hours prior to experimental study. The unit cell cross-section is 20 mm deep to

sufficiently enforce plain strain deformation when the unit is subjected to uniaxial displacement and stress, Figure 1a.

To analyze the electrical and mechanical properties of the metamaterials and units during applied compressive loads, the samples are examined in a load frame (ADMET eXpert 5600, Norwood, Massachusetts) that actuates a rigid platen. A load cell (PCB 110205A, Depew, New York) attached to the upper platen measures the reactive force from the metamaterial as the sample is uniaxially compressed. During compression, a laser displacement sensor (Micro-Epsilon optoNCDT ILD1700-200, Raleigh, North Carolina) identifies the displacement of the platen and, consequently, the top surface of the metamaterial. The resistance of the liquid metal-filled microchannel is monitored using a voltage divider connected to a 5 V source. Data is recorded and processed in a MATLAB program.

2.3 results and Discussion

2.3.1 Conductivity Controlling Mechanism

If constriction is the mechanism by which the electrical conductivity is discretely changed, then it is necessary to assess the relative modes of constriction that may be leveraged. Multiple specimens are fabricated to test the hypothesis of constriction-controlled conductivity. Liquid metal microchannels are embedded in a thin flat plate of silicone rubber, in a solid silicone rubber block of the same net cross-sectional span as the metamaterial unit, and in the X-shaped metamaterial unit, shown in Figure 2a, 2b, and 2c, respectively. The thin flat plate in Figure 2a has length, width, and thickness of 60 mm

(along which the microchannel runs), 30 mm, and 1.5 mm, respectively. The dimensions of the solid rubber block in Figure 2b are 20 mm height, 10 mm width (along which the microchannel runs), and 20 mm depth. The dimensions of the X-shaped metamaterial unit are described in Sec. 2. Each specimen type is fabricated with microchannel diameters of 0.330 mm, 0.460 mm, and 0.737 mm. Each experiment runs for one complete loading cycle, which entails being fully compressed and then uncompressed, with no pauses, at a constant rate of 2 mm per minute. The flat plate is uniaxially compressed with a conical indenter at the location of the microchannel, Figure 1a, while the solid rubber block and X-shaped metamaterial are uniaxially compressed with the flat platen, Figure 1b,c.

The results in Figure 2d relate the applied uniaxial displacement with the resulting stress measured at the respective force indenter or platen for specimens possessing microchannels of 0.737 mm diameter. Despite the conical indentation at the microchannel location, a high stress of nearly 288 kPa is required to eliminate conduction in the flat plate specimen. This is observed around a displacement of 0.723 mm in Figure 2d, where the resistance through the liquid metal trace transitions from around 1 Ω to an open circuit. The analogous events to eliminate conductivity for the solid rubber block and metamaterial unit respectively occur for stresses of 256 kPa and 140 kPa and displacements 6.21 mm and 11.8 mm. The physical deformation of each specimen at the moment of loss of conductivity is depicted in Figures 2a,b,c. Upon removal of the applied displacement, each specimen regains conductivity as evidenced by the loading and unloading arrows to indicate the direction of applied displacement in Figure 2d. These results help to confirm that mechanical constriction of the liquid metal microchannel is

the mechanism to eliminate and recover electrical conductivity regardless of the material embodiment.

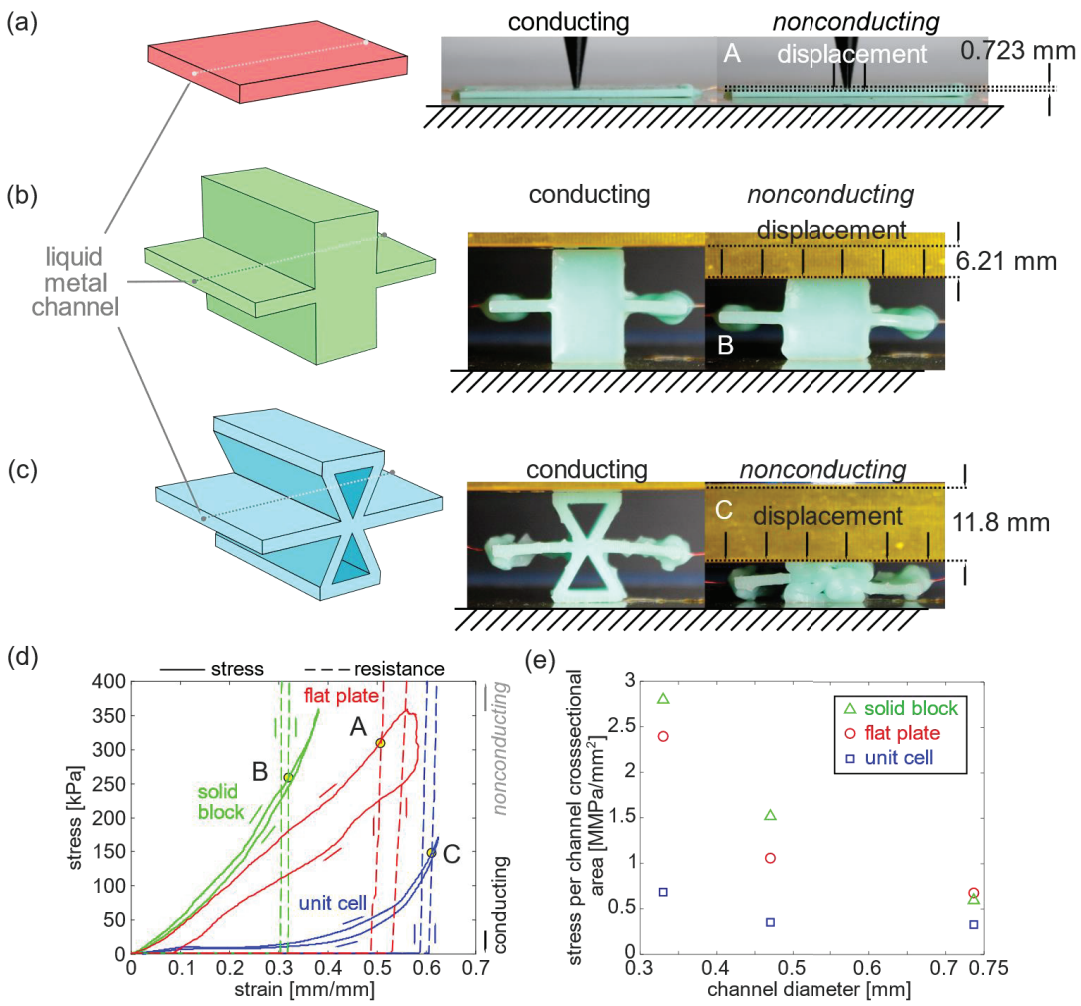

Figure 2. Isometric view displaying embedded microchannel location followed by switching points to open the circuit for the (a) flat plate, (b) solid block, and (c) metamaterial unit cell. (d) Stress resulting from strain as structures and microchannels collapse, and e) influence of host structure and channel diameter on stress required to disconnect the circuit.

A normalized stress measure assists in evaluating the influence of microchannel diameter on the stress activation point corresponding to the loss of conductivity. With the increase of microchannel diameter, the stress per microchannel cross-sectional area required to

disconnect the liquid metal conduction decreases, Figure 2e. Moreover, the results in Figure 2e indicate that the metamaterial unit cell requires less stress per microchannel cross-sectional area to constrict the liquid metal conduit. Since the same mechanism is leveraged in each specimen to eliminate and recover conduction, that is the constriction of the microchannel, the rotation of the unit cell cross-section seen in Figure 1a may therefore play a role to further locally constrict the microchannel than the more uniform deformation fields observed by the flat plate and solid rubber block specimens. Figure 2e also reveals that the range of stresses per microchannel cross-sectional area to constrict conduction decreases as the microchannel diameter increases. This indicates that the microchannel diameter is less influential to control the stress required to constrict conduction as channel diameter increases. In other words, the intricate metamaterial unit cell cross-sectional deformation leads to less variation of cross-section normalized stress to control the digital switching functionality than the use of the same constriction mechanisms in flat plate or solid rubber forms.

The uniaxial effective material modulus (or uniaxial stiffness) is observed from Figure 2d as the slope of the stress-strain profiles. The results reveal that unit cell exhibits varying uniaxial stiffness with change in the applied strain, including slightly negative stiffness after the X-shaped beam networks buckles and rotates, around 0.108 strain. These properties permit favorable functioning in dynamic load environments including vibration and shock [7] [6]. By contrast, the flat plate and solid rubber block exhibit quasi-linear effective uniaxial stiffnesses. As a result, the metamaterial unit cell provides advantageous mechanical properties along with the means to discretely switch the

passage of electrical signals through the unit based on applied stress, a dual-purpose nature not afforded by the counterpart plate and block.

2.3.2 Conductive Switching Longevity

The NaOH used to coat the microchannel prior to injecting liquid metal is discovered to be a vital contributor to longevity of the reversible switching conductivity properties. With exposure to an oxygenated environment, Ga-based liquid metals form an electrically insulative oxide skin. It is established that NaOH inhibits formation of oxide on Ga liquid metals [42]. Here, the influence of NaOH coating in the microchannel is assessed in detail. A unit cell identical to that studied in Section 3.1 with a 0.737 mm diameter microchannel and NaOH emulsion is monitored for a loading and unloading experiment that repeats through 100 cycles. A second unit cell of nominally identical fabrication is used, except no NaOH emulsion is employed prior to injecting the liquid metal. Figure 3a shows the mechanical properties of the applied displacement and resulting stress for all 100 cycles of the unit cell with NaOH emulsion, along with the electrical resistance that fluctuates between conducting at low stress conditions to nonconducting for high stress conditions. The points at which the conduction switches are not at the same stress and displacement conditions for each cycle, although the distinctions are small for the 100 cycles of evaluation. By contrast, the unit cell without the NaOH emulsion shows similar mechanical properties yet does not exhibit consistent switching functionality, as seen in Figure 3b. In fact, only the first 28 of 100 cycles

observe the reversible conduction behavior, after which conduction is permanently terminated.

The stresses at which conduction is switched from conducting to nonconducting states are plotted in Figure 3c as a function of the cycle number. For the case of the 0.737 mm diameter microchannel, the cycle- degradation of the switching functionality is plainly apparent. A staircase-type of trend is observed, as well, to be discussed in the following paragraph. A similarly prolonged working life of the switching functionality is achieved by prewashing an NaOH emulsion for a 0.330 mm diameter microchannel unit cell, seen in Figure 3c. For all cases in Figure 3c, excepting the 0.737 mm microchannel diameter channel unit cell with NaOH emulsion, the sudden loss of conduction follows a steady decline of the stress required to activate the switch functionality. These results suggest that larger microchannel diameters and NaOH emulsions in the microchannels prolong the repeatable switching function of the liquid metal metamaterial units.

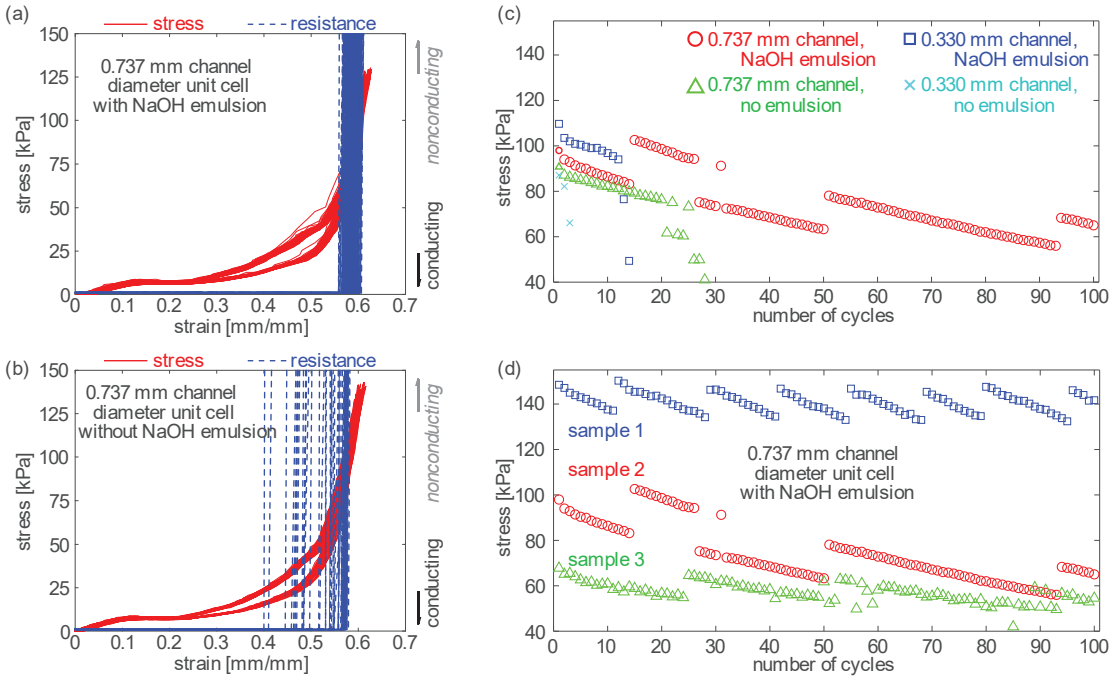

Figure 3. Stress and resistance results of metamaterial unit cells over 100 cycles (a) with NaOH emulsion, and (b) without NaOH emulsion. (c) Stress required to switch from conducting to nonconducting states for different microchannel diameters with and without NaOH emulsion, and (d) iterations of the rise and fall trend of activation stress to induce nonconduction state in larger microchannel diameters.

Measurements for the metamaterial unit with the 0.737 mm diameter liquid metal microchannel with NaOH emulsion show a staircase type pattern in Figure 3c. Three samples of this metamaterial unit are fabricated and independently examined. Each sample exhibits a similar rise and fall trend of the activation stress, with a net decline of the stress required to activate the switch behavior as cycle count increases, Figure 3d. The staircase type trend of switching appears analogous to the stick-slip flow of liquid metal characterized by Larsen et al. [43] associated with formation and breaking of liquid metal

oxide layers in stress-strain cycling. We propose that the same mechanism governs the conductivity of electrical current through the compressed and released microchannel in the metamaterial units examined here by virtue of similar phenomenological stress and strain conditions. Consequently, despite fluctuating stress activation, this study identifies that large microchannel diameters with NaOH emulsion coatings promote long life cycles of electrical switching functionality.

2.3.3 Metamaterial Assembly and Multifunctionality

Given the observations on stress activated conduction in the liquid metal microchannel through the X-shaped unit cell, a metamaterial is fabricated from periodic unit cells that change in beam thickness per layer. Figure 4a presents a schematic of the functionally graded metamaterial, showing beam thicknesses of 1.25 mm, 1.5 mm, and 1.75 mm per layer. The horizontal elastomer segments are 3 mm thick by virtue of containing 1.6 mm perforated polypropylene to reinforce layer by layer compression [10]. Liquid metal microchannels with NaOH emulsions and 0.737 mm diameters are applied as shown in Figure 4a. The electrical conduction through each layer and macroscopic mechanical properties monitored during loading and unloading cycles with results are shown in Figure 4b.

As the metamaterial is uniaxially compressed, the conduction is switched off in the microchannels for the least metamaterial stress at channel 3, followed by channel 2 for slightly greater stress, and then in channel 1 for still further increase in stress. The stresses at which the electrical disconnections occur are 115 kPa, 131 kPa, and 157 kPa,

respectively, for the 3rd, 2nd, and 1st microchannels. During the unloading sequence, the microchannels recover conduction in the reverse order, beginning with channel 1, followed by channel 2, and finally with channel 3. In agreement with the results of Sec. 3.1, the activation of the switching affect in the functionally graded metamaterial appears to be collectively associated with local and global stress in the distinct layers.

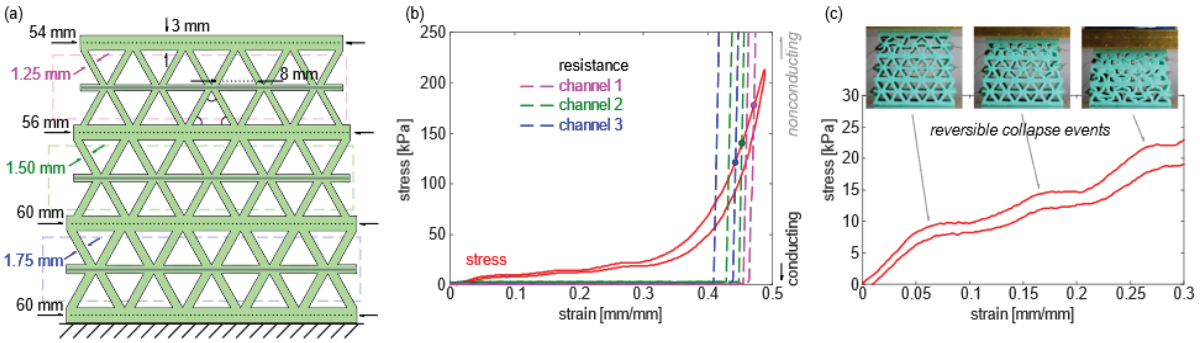

Figure 4. (a) Cross-section of functionally graded metamaterial assembly, (b) changing mechanical and electrical properties resulting from layer-by-layer collapse, and (c) Enlarged view of changing effective uniaxial mechanical properties induced by layer collapse.

The effective uniaxial mechanical properties of the metamaterial are shown in detail in Figure 4c. The results show that collapse of each layer occurs sequentially from the thinnest top layer to the bottom thickest layer. Recovery occurs in the opposite sequence. Because the electrical conduction switching sequence occurs in the opposite layer order for loading and unloading cycles, it may be suggested that the sequence of conduction switching is determined for the functionally graded metamaterial by the stress field

related to the compacted solid. In other words, once all layers collapse in the metamaterial in Figure 4c, the compacted metamaterial exhibits greater stress in the bottom-most layer since the material is quasi-solid. Sec. 3.1 confirmed that solids may also exhibit such electrical switching behaviors, although the metamaterial reduces the absolute stress and relative stress per microchannel cross-sectional area required to induce the switch. As a result, the functionally graded metamaterial exhibits both functional mechanisms that govern conductivity through the liquid metal microchannel.

2.4 Conclusions

In summary, this research furthered the reach and scope of flexible electronics through incorporating liquid metal-filled microchannels into elastomeric structures containing voids to influence structural collapse that can be tailored for sensing and vibration attenuation applications. After proof of concept for a structure that can sense and provide feedback on structural collapse is achieved, the factors inducing microchannel collapse are defined across varying microchannel sizes and host structures. This illuminated that the stress per microchannel cross-sectional area to terminate conduction varies cross-structurally, and decreases with increasing microchannel diameter. Additionally, the lifecycle of conduction for a compression-activated switch, and methods of extending it against the natural growth of oxide layers, is explored. It is demonstrated that such lifecycles may be extended by prewashing the microchannel with NaOH emulsion prior to liquid metal injection, as well as by minimizing the surface-area-to-volume ratio of the microchannel. Finally, a multifunctional metastructure is examined that highlights the

tunable sensing and vibration attenuation capabilities of a stacked structure that utilizes voids to achieve nondestructive and reversible electronic and mechanical property changes. Such discoveries will help pave the way towards a more flexibly powered world.

Chapter 3. Influence of Structural and Magnetoelastic Design on Mechanical Property Control

The ability to finely tune mechanical properties has long been viewed as advantageous across many fields. Some recent methods of achieving such tuning have incorporated magnetic microparticles into elastomeric matrices to create magnetorheological elastomers capable of adapting mechanical properties in real-time with an externally applied magnetic field. Other methods have focused on structural design of lightweight elastomers with void architectures that create mechanical property changes upon collapse. Considering these methods of adapting mechanical properties of a material system, this work integrates these concepts to create a conglomerate of methods by which to tune mechanical properties within a material system. This is initiated through a baseline design of a layered elastomeric metamaterial system containing square void architecture that create consistent, stacked vertical beams. Structural design parameters of these beam ligaments, such as thickness, offset, and combinations thereof, are scrutinized to uncover the individual and combined effects on the collapse of the material system, such as critical force, critical strain, and variable stiffness. Multiple magnetorheological elastomer samples are made using the baseline structural design with different microparticle materials, microparticle poling directions, and applied magnetic field directions to add even greater, in situ tunability to the material system. The result of these numerous methods for altering mechanical properties, during both pre-application

and in situ, is a highly tunable material system with a range of functional mechanical properties for a wide scope of vibration applications.

3.1 Introduction

Emerging research has uncovered the utility of various material systems and applications with tunable mechanical properties, in areas such as hydrogels, biomaterials, and elastomers [44] [45] [46] [47] [48]. One such way to induce mechanical property change is through introducing ferromagnetic particles into an elastomeric matrix to create magnetorheological elastomers (MRE). When subjected to an external magnetic field, MREs experience changes to mechanical properties that may be useful for mitigation in vibration applications [49] [14] [12] [50] [13] [51] [52] [11]. Introducing more than just an external magnetic field for property tuning, Harne et al. [15] incorporate different void architectures into MRE samples to utilize collapse for even greater adaptability than that present in a bulk MRE. These concepts showed the viability of tuning dynamic properties of magnetic metamaterials using applied magnetic fields, pre-strain, and void architectures.

This utilization of void architectures in bulk elastomers to create lightweight elastomer systems has proven to provide shock, impact, and vibration isolation and attenuation [53] [32] [31] [9] [54] [5] [4] [6]. These benefits gained through void architectures are afforded by the deformation and reversible collapse of the elastic beams created by the voids. In an effort to control collapse, El-Helou and Harne [10] examine programmable collapse of elastomeric materials through functionally graded layers of X-shaped beam

networks. By incrementally grading the thickness of the beam networks layer by layer, they are able to control and predict the structural collapse and subsequent changes in mechanical properties. While these methods exemplify individual ways of tuning mechanical properties, there is still much to be explored in combining multiple levels of material system design for multilevel mechanical property adaptability.

Motivated by this prospect, this chapter investigates a tunable material system capable of adapting mechanical properties through both pre-application structural design parameters and in no-contact during application within a magnetic field. The change in mechanical properties are initially accomplished through the utilization of square voids introduced into a bulk elastomer to create beam ligaments capable of reversibly buckling during loading and unloading. Tuning these properties further is achieved through varying structural design parameters of the stacked baseline specimen, namely vertical beam thickness, and offset, Figure 5. During a loading sequence, the combinations of isolated layer increases to beam thicknesses and offsets will affect both the initial stiffness of the material system, and the critical force and critical strain required to induce collapse. For greater tunability, ferromagnetic microparticles are introduced to the elastomeric matrix of the baseline specimen to achieve no-contact stiffness change during loading when a variable magnetic field is present by way of electromagnet.

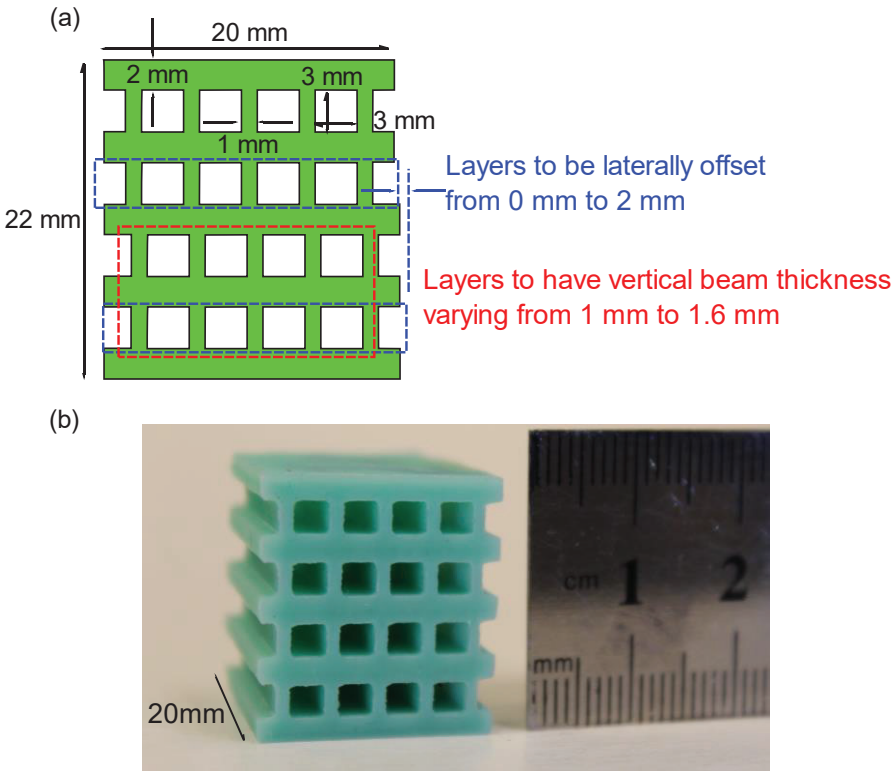

Figure 5. (a) Cross-sectional schematic of baseline specimen that details locations and magnitudes of parameter increases, and (b) a physical baseline specimen.

This chapter studies the layered metamaterial system to identify changes in mechanical properties due to controlled collapse by sequentially increasing beam thickness, offset, and combinations thereof. A finite-element (FE) model is generated to emulate experimental results. Having identified changes to mechanical properties through pre-application structural design parameters, in situ stiffness adaptability is introduced through MRE versions of the baseline specimen with variations in microparticle materials, and poling and field directions. This chapter then concludes with a summary of the discoveries herein and possibilities for future exploration.

3.2 Fabrication and Experimental Methods

3.2.1 Experimental Setup

Throughout this study, the rubber metamaterial systems are fabricated by casting silicone rubber into 3D printed mold negatives of the desired parameters. The 3D printed (FlashForge Creator Pro) molds are produced with acrylonitrile butadiene styrene (ABS) filament. Post mold assembly, platinum cure silicone rubber (Smooth-On Mold Star 15S, Macungie, Pennsylvania) is poured into the mold and left to cure for the recommended 4-hour cure period within atmospheric room conditions. Once demolded, the specimen is left to aerate for 24 hours prior to experimental study. The baseline specimen consists of 4 stacked rows of square voids with 3 mm sides. These voids create consistent and aligned 1 mm thick beam ligaments. Horizontal beams between each row of vertical beams are 2 mm thick to minimize bending during compression. The third and fourth rows of vertical beams, highlighted in red in Figure 5a, experience increases of 0% to 60% to beam thickness at increments of 20% from the baseline thickness of 1 mm. The second and fourth row of vertical beams, highlighted in blue in Figure 5a, experience horizontal offsets of 0 mm to 2 mm in increments of 1 mm. Each combination of the aforementioned parameters are investigated, each maintaining a length, width, and height of 20 mm, 20 mm, and 22 mm, respectively.

The experiments take place within a load frame (ADMET eXpert 5600, Norwood, Massachusetts). The load frame actuates a rigid plate connected to a load cell (PCB 110205A, Depew, New York) which measures reaction forces against the samples during uniaxial compression. In order to monitor displacement, a laser displacement sensor

(Micro-Epsilon optoNCDT ILD1700-200, Raleigh, North Carolina) measures the change in displacement as the top plate is actuated at a constant rate of 0.5 mm per minute. During loading and unloading, all data is recorded and processed in a MATLAB program.

3.2.2 Finite Element Model

Finite element (FE) models were made for the baseline specimen and for each variation of thickness and offset parameters using a dynamic implicit model in ABAQUS. Due to constant cross-sections, 2D plane strain models were utilized to recreate the experimental setup to examine and compare collapse mechanics. A hyperelastic material, Neo-Hookean model was used with the elastomer material properties density, Poisson's ratio, Young's modulus of 1145 $kg.m^{-3}$, 0.499, and 600 kPa, respectively. The bottom plane of each specimen is fixed as to not displace, while the top planes of each specimen are set to linearly displace to a maximum of 9 mm. Each edge of the 2D model is given a self-contact tangential friction penalty of 90% to obtain accurate results upon large collapse resulting in self-contact between beam members. Post-analyses, the reaction forces and displacements on the top plane are extracted to MATLAB.

3.3 Results and Discussion

3.3.1 Variable Structural Design Parameters

The experimental setup is depicted in Figure 6a, showing the fixed bottom boundary, the displacing plate attached to a load cell, and a specimen with 40% thickness and 1 mm offset increase. The resulting experimental and equivalent FE results for force and strain are compared in Figure 6b. It is apparent through both the graphical results and FE strain snapshots that the varying beam thicknesses and offsets create two distinct layers split horizontally through the center cross-section. Each layer experiences discrete buckling events, shown at points 2 and 3. Point 4 displays the point at which the metamaterial system essentially becomes a bulk elastomer. Analyzing the force vs. strain trends, any change in slope indicates a change in uniaxial stiffness of the system.

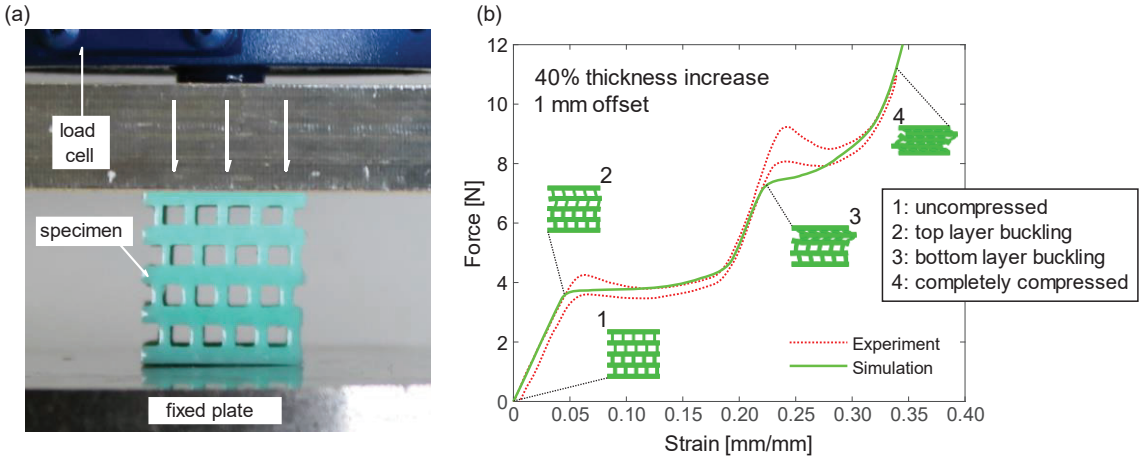

Figure 6. (a) Experimental setup showing a specimen with 40% thickness increase to the third and fourth rows of vertical beams, and 1 mm offset to the second and fourth rows, and (b) comparison of force over strain for experimental and finite element models.

The initial linear stiffness of the FE model closely matches that of the experimental results, depicted by the coincident slopes. Yet, the critical forces and strains vary between these two models. The initial buckling event in the FE model occurs at 3.71 N and 0.0470 mm mm^{-1} strain, while the same event occurs at 4.13 N and 0.0585 mm mm^{-1} in the physical model. Such comparisons and discrepancies are analyzed further for each variation of thickness and offset later in this chapter. Nevertheless, both results indicate multiple regions, including near-zero, of nonlinear stiffness. Such properties are favorable for vibration and shock applications operating with dynamic loads [1].

We first analyze the effect of offsetting the second and fourth rows of vertical beams of the baseline specimen. A visual representation of the offset beams is depicted in Figure 7a. Each level of offset is compared at the different increments of thickness increase, shown in Figure 7b-7e. Prior to any thickness increase, the initial linear stiffness varies across each variation of offset. More specifically, the stiffness decreases as offset increases. This shows that modifying offset alone has the ability to modify mechanical properties of the system. This reduction in stiffness is likely accounted for through the misalignment of stress transfer between the first and second rows of vertical beams, which is only exacerbated with increasingly larger offset. While this trend of varying initial stiffness with increasing offset is maintained across the increasing levels of lower layer beam thickness, the stiffness hierarchy varies across the offsets. This observation can likely be attributed to the dynamic interplay between the combination of offset and beam thickness parameters that affect collapse, and thereby the changing mechanical

properties. Correspondingly, while the buckling events tend to occur at different critical forces, the critical strains at which collapse is induced are generally similar across offsets.

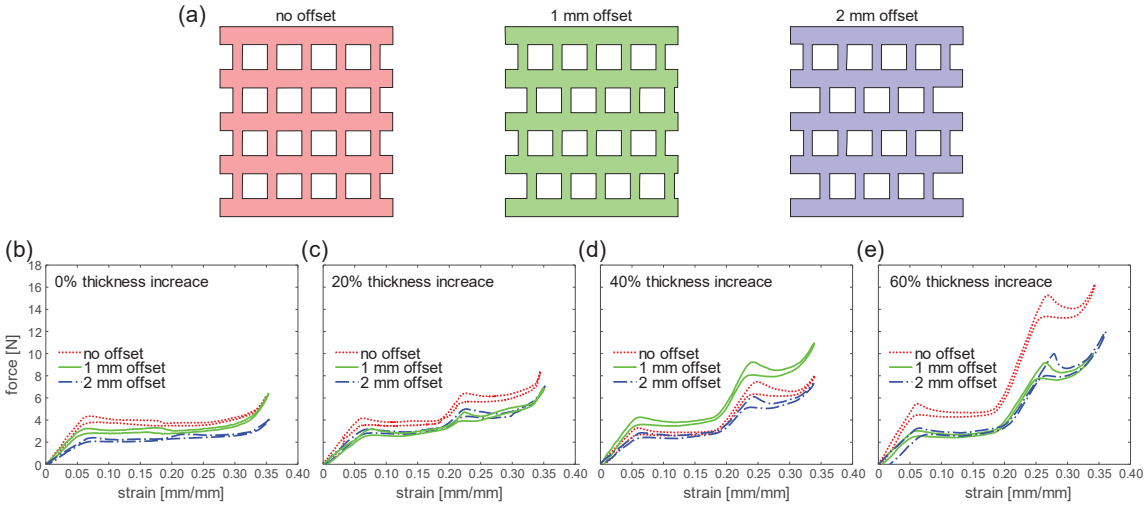

Figure 7. (a) Cross-sectional schematics depicting different levels of offset, and comparisons of force over strain with different levels of offset at (b) 0% thickness increase, (c) 20% thickness increase, (d) 40% thickness increase, and (e) 60% thickness increase.

Also noteworthy is the lack of a distinct second buckling event present in the system with no thickness increase. In this case, all rows of vertical beams act as a single unit that buckle simultaneously. Increasing the thickness of the vertical beams in the third and fourth row, by even 20%, introduces a second distinct buckling event not evident within the baseline thickness. Comparing the different levels of thickness across Figure 7, the hysteresis, or area between the loading and unloading cycles, around the second buckling

point tends to increase as lower level beam thickness increases. This indicates that the increase in beam thickness may also aid in greater energy dissipation within the system [55].

To directly relate the affects of increasing lower layer beam thicknesses, specimens with similar offsets are compared with increasingly thicker vertical beam ligaments, Figure 8. A visual representation of the different levels of thickness increases are depicted in Figure 8a. While the initial pre-buckled stiffness slightly varies as thickness is increased, shown in Figure 8b-8d, it does not have as drastic of an effect as seen in Figure 7.

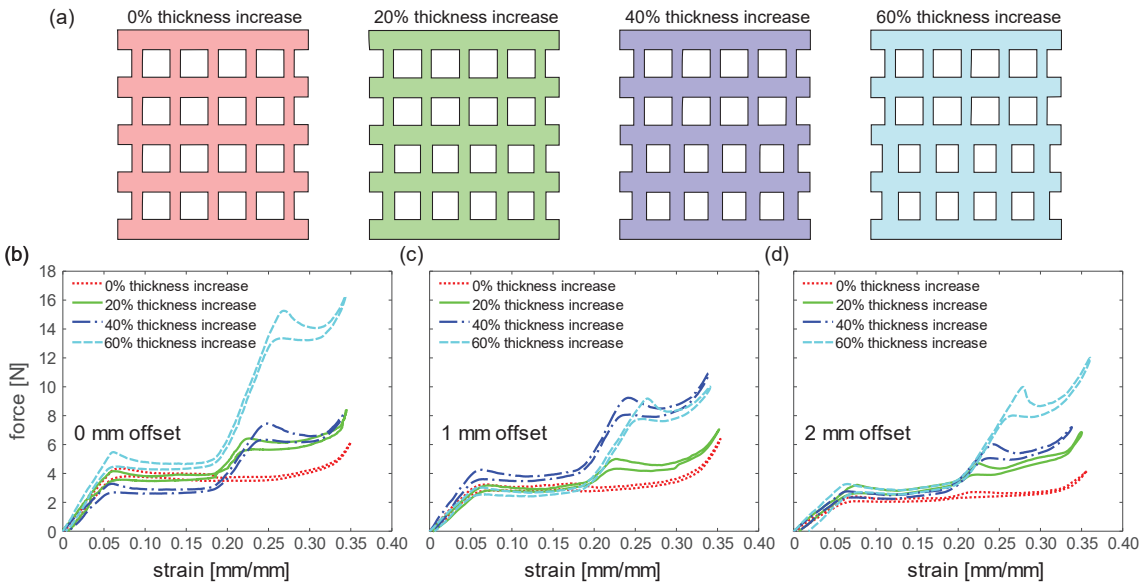

Figure 8. (a) Cross-sectional schematics depicting different levels of thickness increase, and comparisons of force over strain at different levels of thickness increase with (b) 0 mm offset, (c) 1 mm offset, and (d) 2 mm offset.

Similar to the offset comparison, the different levels of thickness increase display similar critical strains for the first buckling event. Unlike the previous comparison, the second buckling events occur at sequentially increasing strain as beam thickness increases. Likewise, these lower layer collapse points also occur at sequentially increasing critical strain with increasing beam thickness, barring a similar critical force between 40% and 60% increase for 1 mm offset. Increasing the lower layer beam thicknesses also shows continually greater negative stiffness immediately after lower level buckling. Since the larger beams require more force to reach the point of buckling, the change in reaction force from the specimen once buckled is more prominent than those with thinner beam ligaments. Another feature present in these comparisons is the increase in strain that the second region of linear stiffness is maintained for prior to the second buckling event. Such traits may be useful in applications with a wider range of variable loading when a constant linear stiffness is desired.

To further scrutinize the discrepancies between the physical and numerical models, the critical force and critical strain values for the first buckling event are gathered in Table 1. The critical values match closely for certain specimens such as the 20% thickness increase with 0 mm offset, and the 0% thickness increase with 1 mm offset having <10% difference in values between FE and experimental results. A few specimens, such as the 60% thickness increase with 0 mm offset, differ >25% between the two models. These results suggest that while the FE model may be capable of providing a designer with a general idea of collapse for some variations of these parameters, better representation of

the material properties within the model are needed for more consistently accurate results across all possible variations.

	FEA		Experimental		|Δ| (% Difference)	
	Force [N]	Strain [mm/mm]	Force [N]	Strain [mm/mm]	|Δ| Force [N]	|Δ| Strain [mm/mm]
0%,0mm	3.71	0.0470	4.13	0.0585	0.42 (10.7%)	0.0115 (21.8%)
20%,0mm	3.97	0.0478	4.02	0.0559	0.05 (1.25%)	0.0081 (15.6%)
40%,0mm	3.97	0.0446	3.17	0.0539	0.80 (22.4%)	0.0093 (18.9%)
60%,0mm	3.98	0.0430	5.25	0.0565	1.27 (27.5%)	0.0135 (27.1%)
0%,1mm	3.31	0.0470	3.12	0.0486	0.19 (5.91%)	0.0016 (3.35%)
20%,1mm	3.35	0.0438	2.79	0.0544	0.56 (18.2%)	0.0106 (21.6%)
40%,1mm	3.52	0.0438	3.86	0.0499	0.34 (9.21%)	0.0061 (13.0%)
60%,1mm	3.46	0.0405	2.78	0.0507	0.68 (21.8%)	0.0102 (22.4%)
0%,2mm	3.04	0.0535	2.31	0.0647	0.73 (27.3%)	0.0112 (19.0%)
20%,2mm	3.24	0.0519	2.93	0.0710	0.31 (10.1%)	0.0191 (31.1%)
40%,2mm	3.27	0.0495	2.73	0.0584	0.54 (18.0%)	0.0089 (16.5%)
60%,2mm	3.28	0.0470	3.14	0.0584	0.14 (4.36%)	0.0114 (21.6%)

Table 1. Comparison of critical force and critical strain to induce the initial buckling event for each changing parameter combination between the finite element analysis and experimental results.

These results, when combined, afford the opportunity for a designer to tune the mechanical properties of this material system for a wide range of dynamic loading applications. By slightly modifying parameters of isolated rows, namely beam thickness and offset, the critical force and strain for multiple collapse events, initial stiffness, magnitude of stiffness change at a buckling point, and durations of linear stiffness are able to be fine-tuned. This controllable malleability of mechanical properties through tuning structural design parameters permits utility for a multitude of vibration attenuation and isolation applications.

3.3.2 In Situ Tuning

Modifying structural design parameters prior to application proved to provide a range of mechanical property tuning capabilities. One disadvantage to this method is that once the material system is designed and fabricated, the range of property changes seen during loading and unloading will be consistent across all cycles. To provide the opportunity for in situ tuning, and providing an even greater range, of mechanical properties, MRE samples of the baseline metamaterial were fabricated and analyzed. Ferromagnetic microparticles, specifically carbonyl iron (CI) (ISP Technologies, Wayne, New Jersey), are mixed into the elastomer at the optimum particle volume fraction of 30% during the casting process [11]. While curing, the samples are placed within the electromagnet to align the particles, creating anisotropic specimens.

An electromagnet was fabricated to provide an external magnetic field around the MRE specimens during loading and unloading, shown in Figure 9. The coil (Buckeye Electrical Products Inc, Botkins, Ohio) of the electromagnet is made with 12 AWG copper wire. At a height of 152.4 mm, the coil has an inner diameter of 50.8 mm, outer diameter of 101.6 mm, and contains 710 turns. The ferromagnetic, 44.5 mm diameter poles of the electromagnet are low carbon steel to attempt to maximize magnetic flux density. The bottom pole is fixed, and designed as to center the specimens within the coil. The top pole is attached to a 152.4 mm long aluminum rod of similar diameter which is attached to the load cell. This extra addition is to create standoff between the loadcell and the field to minimize any possible interference during compression. As the specimen is not visible

during operation due to the encompassing coil, Figure 9 shows the experimental setup with the coil in place on the left, and without the coil on the right.

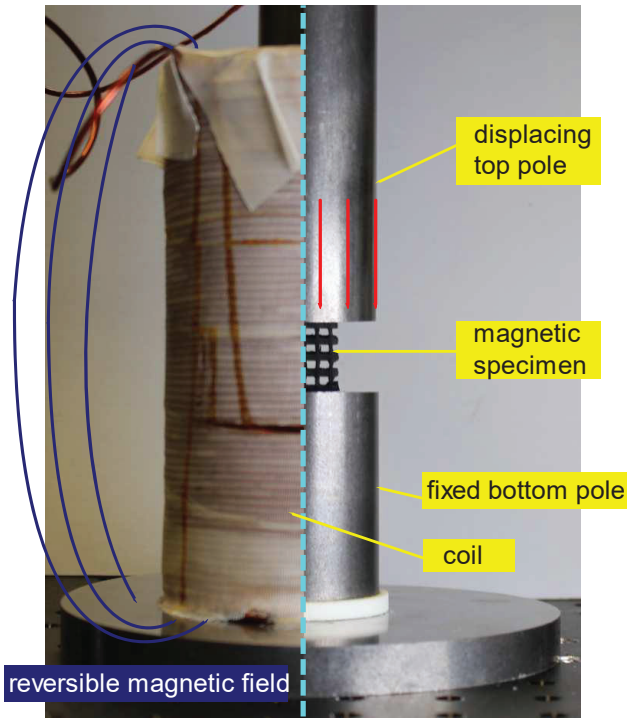

Figure 9. Experimental setup of electromagnet within the load frame for applying an external magnetic field to a specimen during compression. Left: setup with coil surrounding the magnetic specimen. Right: setup prior to coil installation.

By utilizing an electromagnet, the possibility to reverse the field direction by switching the direction of current flow through the coil is available. Taking advantage of this, Figure 10 shows the results of MRE specimens with CI microparticles poled to the left with respect to the front-facing cross-section. The electromagnet is supplied with a

maximum DC current of 5 A during cycling, as to not overheat and destroy the enamel coating on the copper wire. This provides a magnetic flux density of 0.2 T prior to displacement. Prior to cycling the specimens, a loading and unloading sequence was performed with the absence of any specimens to obtain the forces being applied on the load cell by the magnetic field. After acquiring the specimen results, the magnetic force results were subtracted to be able to analyze the mechanical results of the material system.

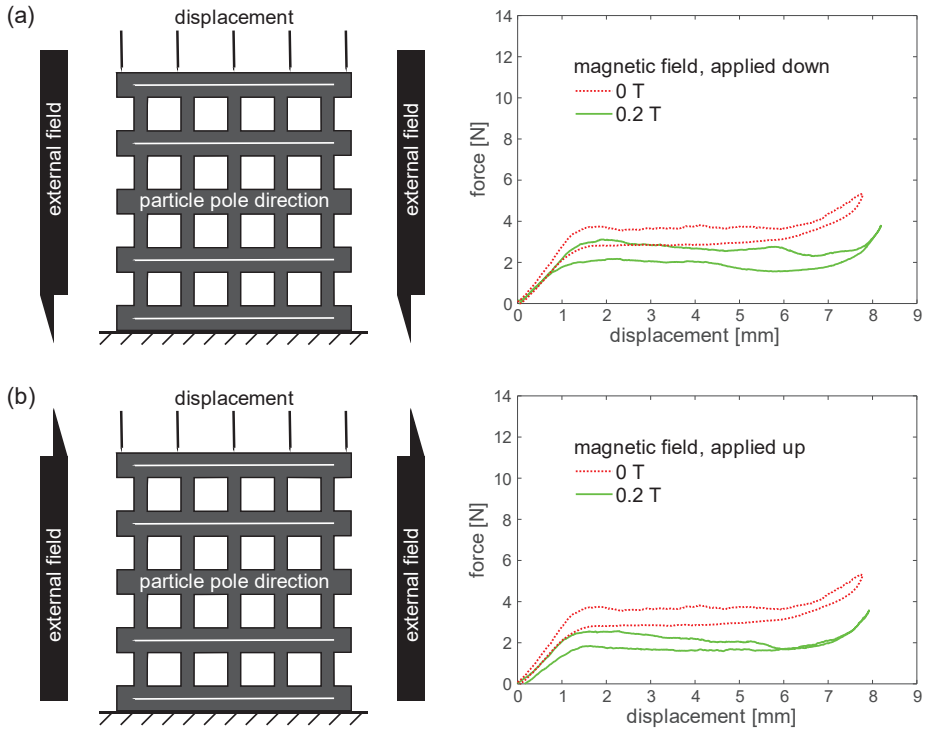

Figure 10. Schematics of baseline specimens fabricated with carbonyl iron microparticles poled leftward during the curing process and cycled with 0 T and 0.2 T external magnetic field applied (a) downward, and (b) applied upward.

The specimen displayed in Figure 10a was cycled with no external magnetic field, and then with external field being applied downward. With field activation, the baseline MRE specimen saw a decrease in stiffness of 19.3%. With the external field direction reversed, the sample in Figure 10b displayed a decrease in stiffness of 21.7%. While both changes in stiffness are similar, both results show a drastic change in stiffness of the baseline structural design parameters. If such MRE samples were to be made with strategic variations of beam thickness and offset, this would give even further tunability to mechanical properties, including in situ, for numerous variable applications.

To examine the effect of different magnetic variables on the baseline MRE specimen, a few more variable samples were examined, with stiffness results displayed in Table 2. Samples A and B are the results from Figure 10a and Figure 10b, respectively. Sample C is similar to Sample A, except sample C had CI microparticles aligned during the curing process using a permanent neodymium magnet. While the electromagnet could only safely achieve a magnetic flux density of 0.2 T, the neodymium magnet provides 0.4 T. This created a stronger alignment of the CI microparticles, resulting in a 3.96% zero field stiffness increase. Once the external field is applied, Sample C experiences an even greater stiffness decrease of 27.7%. To examine if a greater initial stiffness through structural parameters would affect the change in stiffness due to an external field, sample D took the baseline specimen dimensions and increased all vertical beams by 80%, making them 1.8 mm thick.

	A	B	C	D	E	F	G
0T Stiffness [N/m]	2855	2847	2968	5725	3508	6127	3546
0.2T Stiffness [N/m]	2305	2228	2145	5211	3159	5753	3191
Δ Stiffness [N/m]	-550	-619	-823	-514	-349	-374	-355
Δ Stiffness [% change]	-19.3	-21.7	-27.7	-8.98	-9.95	-6.10	-10.0

Table 2. Comparisons of stiffness change with and without an externally applied magnetic field acting upon different baseline samples with A) carbonyl iron microparticles poled leftward with an electromagnet at 0.2 T, cycled with external field applied downward, B) sample A with external field applied upward during loading cycle, C) sample A with microparticles poled leftward with a permanent magnet of 0.4 T, D) sample C with 80% thicker vertical beams, E) sample B using iron oxide microparticles instead of carbonyl iron, F) sample E with microparticles poled downward, and G) sample E with particles poled forward.

While stiffness change within an external field applied downward only saw an 8.98% decrease, the absolute value of the stiffness change is similar to that observed with samples A and B, showing that the larger beams do not inherently increase the effect of the external field on the mechanical properties. Samples E, F, and G were fabricated with 30% vol. iron oxide (IO) (Alpha Chemicals, Missouri) microparticles poled leftward, downward, and forward with respect to the cross-section in the electromagnet. The absolute change in stiffness in these samples were relatively the same, and only about half of that shown in the specimens containing CI. The only notable difference among the IO samples is the initial stiffness of Sample F, where the microparticles were poled downward. This downward poling has the microparticle chains essentially parallel to the uniaxial compression, resulting in much higher initial stiffness. These results show even further in situ tunability of mechanical properties within an already adaptable material system.

3.4 Conclusions

In summary, this chapter explores the design of a highly tunable material system capable of adapting mechanical properties through a multitude of methods. Utilizing stacked layers of vertical beams through the introduction of square voids in a bulk elastomer allows the system to experience different regions of large changes in stiffness, including negative stiffness. These collapse events can be controlled through various pre-application structural design parameter combinations, such as different vertical beam thickness and offsets. Such combinations of changing parameters may dictate critical force and critical strain values for collapse, initial stiffness, duration of linear stiffness, energy dissipated, and magnitude of stiffness change at buckling points. A FE model was established that may give designers a general idea of parameters to induce collapse across different combinations of thickness and offset increase. Even greater tunability of mechanical properties is afforded in the form of in situ stiffness change when introducing ferromagnetic microparticles into the elastomer matrix and cycling the material systems within an external magnetic field. These variables may be investigated even further through more stacked layers of vertical beams, different levels and locations of beam thickness and offset, and stronger magnetic flux density to produce even greater mechanical property changes. These factors combine to create an exceptionally adaptable material system capable of controllable mechanical property tuning through numerous means for a broad range of vibration isolation and attenuation applications.

Chapter 4. Summary and Future Opportunities

Flexible electronics stand out from conventional electronics through the ability to withstand high mechanical strain without loss of electrical functional. This ability is gained through utilizing elastic materials, such as rubbers, and incorporating liquid metal as the conducting path throughout the system. Others have taken advantage of elastomeric metamaterials by using the inherent reversibility of elastic beam buckling for tunable energy dissipation. Yet, research on a combination of these principles to create a flexible electronic metamaterial system to be analyzed under compressive loading to create a conductive switch functionality is lacking.

Likewise, incorporating magnetic microparticles into an elastomer matrix to create magnetorheological elastomers has been proven to affect the mechanical properties of such a system both with and outside of an externally applied magnetic field. Introductory research has already been undertaken to establish the utility of combining these principles with void architectures to create lightweight, magnetically susceptible metamaterials. Existing research scrutinizes individual structural design properties of lightweight metamaterials. Yet, research combining multiple of these collapse-controlling parameters is lacking.

Motivated by this lack of knowledge in the fields of engineering and material science, the research herein sought to achieve the objectives proposed in chapter 1, with the findings

stated in this chapter. After acknowledging the successful realization of the objectives, future research opportunities that utilize the findings herein are proposed.

4.1 Research Findings

4.1.1 Development of a Flexible Electronic Metamaterial that Modifies Conductive State Through Collapse

This research sought to develop an elastomeric metamaterial system that incorporates liquid metal-filled microchannels such that the state of conduction may be affected during collapse. A novel flexible electronic metamaterial was developed herein with inherent conductive state-switching functionality. This switching of conductive state was accomplished through the rotational buckling and collapse of the X-shaped beam network, displayed in Figure 1, which induces constriction of the liquid metal-filled microchannel, thereby terminating conduction. Due to the reversibility of the elastic buckling beams and the fluidity of the liquid metal, this novel functionality was able to achieve repeatable switching off and on of conduction through compressive loading. This functionality provided a foundation upon which further research may illuminate the mechanism of stress-induced microchannel collapse for sensing capabilities.

4.1.2 Relationships Between Structural and Microchannel Deformation for Sensing Capabilities

Once a device capable of utilizing reversible mechanical collapse to reversibly change conductive state was conceived, an understanding of the microchannel collapsing mechanism was needed. To illuminate the mechanics behind microchannel collapse, liquid metal-filled microchannels were embedded in various structures, with various microchannel diameters. This uncovered that the stress per cross-sectional area of the microchannel to induce constriction to the point of opening the circuit and switching off conduction is dependent upon both the host structure, and microchannel diameter. Furthermore, methods of mitigating the natural buildup of nonconductive oxide layers on the surface of the liquid metal was explored to extend conductive state switching functionality. It was found that this functionality may stay intact for longer lifecycles by prewashing the microchannel with NaOH emulsion prior to liquid metal injection, and by utilizing larger microchannel diameters to minimize the surface-area-to-volume ratio of the microchannel. Finally, these findings were incorporated into a stacked, functionally graded metamaterial containing filled microchannels within each layer. This system accentuated the multistep sensing capabilities through sequential channel disconnection at increasingly higher stress, combined with the layer-by-layer buckling inducing mechanical property changes. These findings lay the groundwork for flexible electronics with control of compression-activated conductive switches for sensing and mechanical property adapting multifunctionality.

4.1.3 Influence of Structural and Magnetoelastic Design on Mechanical Property Control

The undertaking of this research sought to utilize the combination of multiple structural design parameters and an external magnetic field to identify the influence on mechanical properties of a magnetoelastic metamaterial. In doing so, it was found in chapter 3 that the initial linear stiffness may be sequentially decreased simply by increasing offset between layers of vertical beams. While this trend of altering pre-buckled stiffness is maintained when introducing thickness increases in tandem with offset, it becomes less accentuated due to the interplay between the parameters. Notably, the buckling points across each offset generally have similar critical strain, while the critical force varies. However, increasing beam thickness, consistent across all offsets, results in sequentially increasing critical strain to induce secondary buckling of the lower metamaterial layer. Likewise, similar results are seen in the critical force for secondary buckling with beam thickness increase. Unlike the offset increases, increasing the beam thickness results in both increasingly more stiffness change upon secondary buckling, and maintains the secondary linear stiffness for increasingly longer strains. The introduction of in situ mechanical property changes through multiple methods of incorporating ferromagnetic microparticles into the baseline specimen were then scrutinized, enabling in situ stiffness changes as high as 27.7%. The combination of these parameters displayed a highly tunable material system that gives way to control critical force and critical strain values of collapse, initial stiffness, duration of linear stiffness, energy dissipated, magnitude of stiffness change at buckling points, and in situ stiffness control.

4.2 Future Research Avenues

4.2.1 Complex Microchannel Networks

This research reveals methods of controlling collapse of singular, nonconnected liquid metal-filled microchannels. These findings have developed groundwork from which more complex microchannel networking may be established. The metamaterial system examined herein, while able to sense different loadings through nonconnected, stacked microchannels, are only able to sense uniaxial deformation. Similar metamaterials as those analyzed in chapters 2 and 3 that incorporate networks of liquid metal-filled microchannels in not only the horizontal beam ligaments, but also the vertical and diagonal beams may allow multiple levels of multiaxial sensing. A unique fabrication method would be necessary to strategically implement such complex networks of microchannels, as the method used in this research is only simply applied to single-microchannel structures. One way of achieving such network complexity may be to directly print the elastomer, enabling easy and instant microchannel creation upon curation [32]. Filling these complex microchannel networks would also require more than simply using a syringe to inject the liquid metal, such as using vacuum filling techniques to fully fill each path, or steering the liquid metal with low voltages [56]. Such a system may become as complex as imaginable, incorporating many individual networks through differently oriented beams, through the cross-section, make radial turns, or entirely fill the system [57]. This highly complex system may be capable of sensing pinpoint locations of certain stress thresholds, while also maintaining the advantageous changes in mechanical properties.

4.2.2 Accurate Modeling of Magnetorheological Metamaterial

A model was presented in chapter 2 that gave a general idea of the critical force and critical strain to induce collapse of the metamaterial system at different levels of thickness and offset increase. While such a model may account for structural design properties, it is unable to account for the magnetic-mechanical coupling taking place within the specimens containing magnetic microparticles. While elementary modeling of a unit cell of a microparticle embedded in elastomer has been achieved, an accurate model of systems analyzed in this research requires high nonlinearity [11]. Due to the high nonlinearity inherent in such systems, this would require a highly complex, and computational heavy model to achieve [58]. Preliminary insight has been gained on this through exploring co-simulation within a software capable of handling nonlinearity, such as ANSYS. It seems that such a model may be possible through creating a co-simulation between ANSYS Maxwell and ANSYS Static Structural analysis systems [59]. Such a model would require a 3D model with independent boundary conditions within each respective analysis system. An iterative setup would then need to be established between the two systems to incrementally share their respective results, as each increment of mechanical displacement will affect the microparticle orientation and flux density within Maxwell. Likewise, each increment of microparticle orientation and flux density will affect the mechanical reaction forces on the top layer of the structure. Such an iterative process will require intricate 3D modeling that accurately represents the microparticle dispersion and alignment, along with miniscule step sizes to fully and accurately represent this type of system. This type of modelling may provide methods for furthering

this type of magnetic-mechanical coupling at high magnetic flux densities without the inherent hazards present in strong magnetic fields.

4.2.3 Incorporating Liquid Metal-filled Microchannels into Magnetorheological Metamaterials

This research studies the utility of individually incorporated different forms of metal into elastomeric material systems. While each method has shown benefits in ability to affect mechanical and/or electrical properties of the system, these principles may be combined to create a novel material system with even greater functionality [60] [61] . Take, for instance, the baseline specimen containing carbonyl iron microparticles studied in chapter 3, and embed liquid metal-filled microchannels within the horizontal beam ligaments. Such a system would contain the sensing capabilities presented in chapter 2, with the susceptibility to changing mechanical properties induced by an externally applied magnetic field, as presented in chapter 3. Utilizing understanding of mechanical collapse affected by pre-structural design parameters and magnetic particle integration, a complex controls setup may be implemented such that corrective feedback provided by the conduction states of the horizontal beams at different levels of collapse may alter the external magnetic field [62]. This alteration to the magnetic field may then affect the instantaneous mechanical properties of the material system. This iterative corrective feedback essentially creates an autonomous, self-tuning material system capable of sensing current loading, and subsequently changing the magnetic field to achieve desired

mechanical properties [63]. Such a system would provide unprecedented capabilities for self-adaptation within a range of vibration applications.

References

[1] R. Harne and K. Wang, Harnessing bistable structural dynamics: for vibration control, energy harvesting and sensing, John Wiley & Sons, 2017.

[2] S. Babaee, J. Shim, J. Weaver, E. Chen, N. Patel and K. Bertoldi, "3D soft metamaterials with negative Poisson's ratio," *Advanced Materials,* vol. 25, pp. 5044-5049, 2013.

[3] K. Bertoldi, P. Reis, S. Willshaw and T. Mullin, "Negative poisson's ratio behavior induced by an elastic instability," *Advanced Materials,* vol. 22, pp. 361-366, 2010.

[4] T. Frenzel, C. Findeisen, M. Kadic, P. Gumbsch and M. Wegener, "Tailored buckling microlattices as reusable light-weight shock absorbers," *Advanced Materials,* vol. 28, pp. 5865-5870, 2016.

[5] J. Bishop, Q. Dai, Y. Song and R. Harne, "Resilience to impact by extreme energy absorption in lightweight material inclusions constrained near a critical point," *Advanced Engineering Materials,* vol. 18, pp. 1871-1876, 2016.

[6] P. Vuyk, S. Cui and R. Harne, "Illuminating origins of impact energy dissipation in mechanical metamaterials," *Advanced Engineering Materials,* vol. 20, p. 1700828, 2018.

[7] D. Restrepo, N. Mankame and P. Zavattieri, "Phase transforming cellular materials," *Extreme Mechanics Letters,* vol. 4, pp. 52-60, 2015.

[8] J. Meaud and K. Che, "Tuning elastic wave propagation in multistable architected materials," *International Journal of Solids and Structures,* vol. 122, pp. 69-80, 2017.

[9] S. Cui and R. Harne, "Characterizing the nonlinear response of elastomeric material systems under critical point constraints," *International Journal of Solids and Structures,* vol. 135, pp. 197-207, 2018.

[10] C. El-Helou and R. Harne, "Exploiting functionally graded elastomeric materials to program collapse and mechanical properties," *Advanced Engineering Materials,* vol. 21, p. 1900807, 2019.

[11] L. C. Davis, "Model of magnetorheological elastomers," *Journal of Applied Physics,* vol. 85, pp. 3348-3351, 1999.

[12] X. Guan, X. Dong and J. Ou, "Magnetostrictive effect of magnetorheological elastomer," *Journal of Magnetism and Magnetic Materials,* vol. 320, pp. 158-163, 2008.

[13] M. Behrooz, X. Wang and F. Gordaninejad, "Performance of a new magnetorheological elastomer isolation system," *Smart Materials and Structures,* vol. 23, p. 045014, 2014.

[14] M. Kallio, T. Lindroos, S. Aalto, E. Järvinen, T. Kärnä and T. Meinander, "Dynamic compression testing of a tunable spring element consisting of a magnetorheological elastomer," *Smart Materials and Structures,* vol. 16, pp. 506-514, 2007.

[15] R. Harne, Z. Deng and M. Dapino, "Adaptive magnetoelastic metamaterials: a new class of magnetorheological elastomers," *Journal of Intelligent Material Systems and Structures,* vol. 29, pp. 265-278, 2018.

[16] Y. Kim, H. Yuk, R. Zhao, S. Chester and X. Zhao, "Printing ferromagnetic domains for untethered fast-transforming soft materials," *Nature,* vol. 558, pp. 274-279, 2018.

[17] S. Aziz, S. Mazlan, N. Nik Ismail, Ubaidillah, M. Khairi and N. Yunus, "Rheological properties of carbon nanotubes-reinforced magnetorheological elastomer," *Journal of Physics: Conference Series,* vol. 795, p. 012074, 2017.

[18] L. Chen, X. Gong and W. Li, "Effect of carbon black on the mechanical performances of magnetorheological elastomers," *Polymer Testing,* vol. 27, pp. 340-345, 2008.

[19] M. Dickey, "Stretchable and soft electronics using liquid metals," *Advanced Materials,* vol. 29, p. 1606425, 2017.

[20] N. Lu, C. Lu, S. Yang and J. Rogers, "Highly sensitive skin-mountable strain gauges based entirely on elastomers," *Advanced Functional Materials,* vol. 22, pp. 4044-4050, 2012.

[21] S. Xu, Y. Zhang, L. Jia, K. Mathewson, K. Jang, J. Kim, H. Fu, X. Huang, P. Chava, R. Wang and S. Bhole, "Soft microfluidic assemblies of sensors, circuits, and radios for the skin," *Science,* vol. 344, pp. 70-74, 2014.

[22] F. Suarez, D. Parekh, C. Ladd, D. Vashaee, M. Dickey and M. Öztürk, "Flexible thermoelectric generator using bulk legs and liquid metal interconnects for wearable electronics," *Applied Energy,* vol. 202, pp. 736-745, 2017.

[23] J. Boley, E. White and R. Kramer, "Mechanically sintered gallium–indium nanoparticles," *Advanced Materials,* vol. 27, pp. 2355-2360, 2015.

[24] J. Boley, E. White, G. Chiu and R. Kramer, "Direct writing of gallium-indium alloy for stretchable electronics," *Advanced Functional Materials,* vol. 24, pp. 3501-3507, 2014.

[25] A. Diebold, A. Watson, S. Holcomb, C. Tabor, D. Mast, M. Dickey and J. Heikenfeld, "Electrowetting-actuated liquid metal for RF applications," *Journal of Micromechanics and Microengineering,* vol. 27, p. 025010, 2017.

[26] Z. Farrell and C. Tabor, "Control of gallium oxide growth on liquid metal eutectic gallium/indium nanoparticles via thiolation," *Langmuir,* vol. 34, pp. 234-240, 2018.

[27] S. Holcomb, M. Brothers, A. Diebold, W. Thatcher, D. Mast, C. Tabor and J. Heikenfeld, "Oxide-free actuation of gallium liquid metal alloys enabled by novel acidified siloxane oils," *Langmuir,* vol. 32, pp. 12656-12663, 2016.

[28] M. Dickey, "Emerging applications of liquid metals featuring surface oxides," *ACS Applied Materials & Interfaces,* vol. 6, pp. 18369-18379, 2014.

[29] E. Markvicka, M. Bartlett, X. Huang and C. Majidi, "An autonomously electrically self-healing liquid metal-elastomer composite for robust soft-matter robotics and electronics," *Nature Materials,* vol. 17, pp. 618-624, 2018.

[30] B. Blaiszik, A. Jones, N. Sottos and S. White, "Microencapsulation of gallium–indium (Ga–In) liquid metal for self-healing applications," *Journal of Microencapsulation,* vol. 31, pp. 350-354, 2014.

[31] N. Sears, J. Berrigan, P. Buskohl and R. Harne, "Dynamic response of flexible hybrid electronic material systems," *Composite Structures,* vol. 208, pp. 377-384, 2019.

[32] N. Sears, J. Berrigan, P. Buskohl and R. Harne, "Flexible hybrid electronic material systems with programmable strain sensing architectures," *Advanced Engineering Materials,* vol. 20, p. 1800499, 2018.

[33] C. Majidi, R. Kramer and R. Wood, "A non-differential elastomer curvature sensor for softer-than-skin electronics," *Smart Materials and Structures,* vol. 20, p. 105017, 2011.

[34] J. Muth, D. Vogt, R. Truby, Y. Mengüç, D. Kolesky, R. Wood and J. Lewis, "Embedded 3D printing of strain sensors within highly stretchable elastomers," *Advanced Materials,* vol. 26, pp. 6307-6312, 2014.

[35] C. Pang, G. Lee, T. Kim, S. Kim, H. Kim, S. Ahn and K. Suh, "A flexible and highly sensitive strain-gauge sensor using reversible interlocking of nanofibres," *Nature Materials,* vol. 11, pp. 795-801, 2012.

[36] A. Valentine, T. Busbee, J. Boley, J. Raney, A. Chortos, A. Kotikian, J. Berrigan, M. Durstock and J. Lewis, "Hybrid 3D printing of soft electronics," *Advanced Materials,* vol. 29, p. 1703817, 2017.

[37] B. Blaiszik, S. Kramer, M. Grady, D. McIlroy, J. Moore, N. Sottos and S. White, "Autonomic restoration of electrical conductivity," *Advanced Materials,* vol. 24, pp. 398-401, 2012.

[38] C. Thrasher, Z. Farrell, N. Morris, C. Willey and C. Tabor, "Mechanoresponsive polymerized liquid metal networks," *Advanced Materials,* vol. 31, p. 1903864, 2019.

[39] A. Fassler and C. Majidi, "Liquid-phase metal inclusions for a conductive polymer composite," *Advanced Materials,* vol. 27, pp. 1928-1932, 2015.

[40] M. Ford, C. Ambulo, T. Kent, E. Markvicka, C. Pan, J. Malen, T. Ware and C. Majidi, "A multifunctional shape-morphing elastomer with liquid metal inclusions," *Proceedings of the National Academy of Sciences,* vol. 116, pp. 21438-21444, 2019.

[41] J. Bunyan and S. Tawfick, "Exploiting structural instability to design architected materials having essentially nonlinear stiffness," *Advanced Engineering Materials,* vol. 21, p. 1800791, 2019.

[42] R. Bilodeau, D. Zemlyanov and R. Kramer, "Liquid metal switches for environmentally responsive electronics," *Advanced Materials Interfaces,* vol. 4, p. 1600913, 2017.

[43] R. Larsen, M. Dickey, G. Whitesides and D. Weitz, "Viscoelastic properties of oxide-coated liquid metals," *Journal of Rheology,* vol. 53, pp. 1305-1326, 2009.

[44] L. Wang, J. Chung, P. Chan and M. Kurisawa, "Injectable biodegradable hydrogels with tunable mechanical properties for the stimulation of neurogenesic differentiation of human mesenchymal stem cells in 3D culture," *Biomaterials,* vol. 31, pp. 1148-1157, 2010.

[45] S. Seidlits, Z. Khaing, R. Petersen, J. Nickels, J. Vanscoy, J. Shear and C. Schmidt, "The effects of hyaluronic acid hydrogels with tunable mechanical properties on neural progenitor cell differentiation," *Biomaterials,* vol. 31, 2010.

[46] D. Coutinho, S. Sant, H. Shin, J. Oliveira, M. Gomes, N. Neves, A. Khademhosseini and R. Reis, "Modified gellan gum hydrogels with tunable physical and mechanical properties," *Biomaterials,* vol. 31, pp. 7494-7502, 2010.

[47] J. Stampfl, S. Baudis, C. Heller, R. Liska, A. Neumeister, R. Kling, A. Ostendorf and M. Spitzbart, "Photopolymers with tunable mechanical properties processed by laser-based high-resolution stereolithography," *Journal of Micromechanics and Microengineering,* vol. 18, p. 125014, 2008.

[48] L. Li, S. Teller, R. Clifton, X. Jia and K. Kiick, "Tunable mechanical stability and deformation response of a resilin-based elastomer," *Biomacromolecules,* vol. 12, pp. 2302-2310, 2011.

[49] H. Deng and X. Gong, "Adaptive tuned vibration absorber based on magnetorheological elastomer," *Journal of Intelligent Material Systems and Structures,* vol. 18, pp. 1205-1210, 2007.

[50] G. Zhou and Z. Jiang, "Deformation in magnetorheological elastomer and elastomer–ferromagnet composite driven by a magnetic field," *Smart Materials and Structures,* vol. 13, p. 309, 2004.

[51] Y. Li, J. Li, W. Li and B. Samali, "Development and characterization of a magnetorheological elastomer based adaptive seismic isolator," *Smart Materials and Structures,* vol. 22, p. 035005, 2013.

[52] J. Yang, S. Sun, H. Du, W. Li, G. Alici and H. Deng, "A novel magnetorheological elastomer isolator with negative changing stiffness for vibration reduction," *Smart Materials and Structures,* vol. 23, p. 105023, 2014.

[53] S. Yeh and R. Harne, "Tailoring concurrent shear and translational vibration control mechanisms in elastomeric metamaterials for cylindrical structures," *Mechanical Systems and Signal Processing,* vol. 117, pp. 609-633, 2018.

[54] J. Shim, S. Shan, A. Košmrlj, S. Kang, E. Chen, J. Weaver and K. Bertoldi, "Harnessing instabilities for design of soft reconfigurable auxetic/chiral materials," *Soft Matter,* vol. 9, pp. 8198-8202, 2013.

[55] N. Kidambi, R. Harne and K. Wang, "Adaptation of energy dissipation in a mechanical metastable module excited near resonance," *Journal of Vibration and Acoustics,* vol. 138, p. 011001, 2016.

[56] S. Tang, Y. Lin, I. Joshipura, K. Khoshmanesh and M. Dickey, "Steering liquid metal flow in microchannels using low voltages," *Lab on a Chip,* vol. 15, pp. 3905-3911, 2015.

[57] S. Liang, Y. Li, Y. Chen, J. Yang, T. Zhu, D. Zhu, C. He, Y. Liu, S. Handschuh-Wang and X. Zhou, "Liquid metal sponges for mechanically durable, all-soft, electrical conductors," *Journal of Materials Chemistry C,* vol. 5, pp. 1586-1590, 2017.

[58] R. Sheridan, J. Roche, S. Lofland and P. vonLockette, "Numerical simulation and experimental validation of the large deformation bending and folding behavior of magneto-active elastomer composites," *Smart Materials and Structures,* vol. 23, p. 094004, 2014.

[59] Y. Li and J. Li, "Finite element design and analysis of adaptive base isolator utilizing laminated multiple magnetorheological elastomer layers," *Journal of Intelligent Material Systems and Structures,* vol. 26, pp. 1861-1870, 2015.

[60] B. Ma, C. Xu, J. Chi, J. Chen, C. Zhao and H. Liu, "A versatile approach for direct patterning of liquid metal using magnetic field," *Advanced Functional Materials,* vol. 29, p. 1901370, 2019.

[61] J. Jeon, J. Lee, S. Chung and D. Kim, "On-demand magnetic manipulation of liquid metal in microfluidic channels for electrical switching applications," *Lab on a Chip,* vol. 17, pp. 128-133, 2017.

[62] M. Rakotondrabe, I. Ivan, S. Khadraoui, P. Lutz and N. Chaillet, "Simultaneous displacement/force self-sensing in piezoelectric actuators and applications to robust control," *IEEE/ASME Transactions on Mechatronics,* vol. 20, pp. 519-531, 2014.

[63] C. Lan and C. Fan, "An accurate self-sensing method for the control of shape memory alloy actuated flexures," *Sensors and Actuators A: Physical,* vol. 163, pp. 323-332, 2010.